

Flanders
State of
the Art

15_112_1
FHR reports

Validation of SPH-based model for sea walls with horizontal cantilever slab

Final Report

Validation of SPH-based model for sea walls with horizontal cantilever slab

Final Report

Altomare, C.; González-Cao, J.; Crespo, A.J.C.; Domínguez, J.M.; Vanneste, D.; Peeters, P.; Mostaert, F.

Legal notice

Flanders Hydraulics Research is of the opinion that the information and positions in this report are substantiated by the available data and knowledge at the time of writing.

The positions taken in this report are those of Flanders Hydraulics Research and do not reflect necessarily the opinion of the Government of Flanders or any of its institutions.

Flanders Hydraulics Research nor any person or company acting on behalf of Flanders Hydraulics Research is responsible for any loss or damage arising from the use of the information in this report.

Copyright and citation

© The Government of Flanders, Department of Mobility and Public Works, Flanders Hydraulics Research 2017
D/ 2017/3241/97

This publication should be cited as follows:

Altomare, C.; González-Cao, J.; Crespo, A.J.C.; Domínguez, J.M.; Vanneste, D.; Peeters, P.; Mostaert, F. (2017). Validation of SPH-based model for sea walls with horizontal cantilever slab: Final Report. Version 2.0. FHR Reports, 15_112_1. Flanders Hydraulics Research: Antwerp.


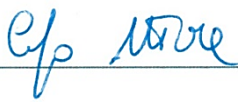
Reproduction of and reference to this publication is authorised provided the source is acknowledged correctly.

Document identification

| | | | |
|------------------|--|--|-----------------|
| Customer: | Flanders Hydraulics Research | Ref.: | WL2017R15_112_1 |
| Keywords (3-5): | SPH, wave forces, cantilever | | |
| Text (p.): | 20 | Appendices (p.): | / |
| Confidentiality: | <input checked="" type="checkbox"/> No | <input checked="" type="checkbox"/> Available online | |

| | |
|------------|--|
| Author(s): | Altomare, C.; González-Cao, J.; Crespo, A.J.C.; Domínguez, J.M.; |
|------------|--|

Control

| | Name | Signature |
|-----------------|--------------|--|
| Reviser(s): | Vanneste, D. |  |
| Project leader: | Altomare, C. |  |

Approval

| | | |
|-----------------------------|--------------|--|
| Coordinator research group: | Peeters, P. |  |
| Head of Division: | Mostaert, F. |  |

Abstract

The capability of the meshless model DualSPHysics to reproduce violent wave impacts on sea walls with horizontal cantilever slabs is assessed. Physical model tests were carried out at Ghent University using monochromatic waves with different wave conditions at the toe of the structure. The free-surface elevation along the flume and the forces exerted onto the vertical part of the structure obtained with DualSPHysics were compared with experimental measurements, showing a good accuracy. In addition, both the efficiency and reliability of DualSPHysics were compared with those of IHFOAM, which is a state-of-the-art mesh-based model. Both models have shown a similar performance and accuracy, which suggests that meshless methods have attained the required level of maturity to be used for engineering purposes.

The present report includes and integrates the work contained in a research paper submitted for publication to Computers & Fluids.

Contents

| | |
|--|-----|
| Abstract | III |
| Contents | v |
| List of tables..... | vi |
| List of figures | vii |
| 1 Introduction..... | 1 |
| 2 Numerical models..... | 3 |
| 2.1 DualSPHysics model..... | 3 |
| 2.2 IHFOAM | 4 |
| 3 Case of study | 5 |
| 3.1 The physical model..... | 5 |
| 3.2 Wave conditions | 6 |
| 4 Results and discussion | 8 |
| 4.1 Wave shape development..... | 8 |
| 4.2 Free-surface elevation..... | 9 |
| 4.3 Wave forces onto vertical wall | 12 |
| 4.4 Uplift wave forces..... | 14 |
| 4.5 Sensitivity analysis of the numerical models to spatial resolution | 15 |
| 4.6 Model efficiency | 15 |
| 5 Conclusions..... | 17 |
| References..... | 18 |

List of tables

Table 1. Distance (m) to the wave gauges measured from wave paddle. 6

Table 2. Distance (m) from the toe of the structure to the pressure sensors located on the vertical wall and distance from the vertical wall to the pressure sensors located on the horizontal wall (see Figure 1) 6

Table 3. Wave conditions 6

Table 4. Skill index calculated for wave elevation at 8 gauges. Mean and standard deviation of the skill index was also calculated using the value of the index at every gauge for every wave (last two rows). 12

Table 5. Skill index for the horizontal force of DualSPHysics and IHFOAM models. 14

List of figures

| | |
|--|----|
| Figure 1. Setup of the experiment..... | 5 |
| Figure 2. Discretization of a square domain of size $L \times h$ using DualSPHysics and IHFOAM where $dp=dx$ and $N_p \approx N_c$ | 7 |
| Figure 3. Different instants of the DualSPHysics and IHFOAM simulations of Wave#2 compared with the experimental wave profiles (red dots). | 9 |
| Figure 4. Time series of numerical (DualSPHysics and IHFOAM) and experimental free-surface elevation for Wave#2 case at WG1 and WG7..... | 10 |
| Figure 5. Taylor's diagrams with comparison of numerical free-surface elevations for DualSPHysics (red numbers) and IHFOAM (blue numbers) using the experimental free-surface elevation as reference (Ref).. | 11 |
| Figure 6. Time series of the numerical (DualSPHysics and IHFOAM) and experimental horizontal force exerted against the vertical wall of the structure for Wave#2. | 13 |
| Figure 7. Taylor diagram with comparison of numerical horizontal force for DualSPHysics (red) and IHFOAM (blue) using the experimental free-surface elevation as reference (Ref). | 13 |
| Figure 8. Time series of the numerical (DualSPHysics and IHFOAM) and experimental uplift forces exerted against the horizontal slab for Wave#2..... | 14 |
| Figure 9. Taylor diagram with sensitivity analysis to resolution of free-surface elevation at WG7 (left panel) and horizontal force onto the vertical wall (right panel) with DualSPHysics and IHFOAM for Wave #2..... | 15 |
| Figure 10. Computational times for the different simulations using IHFOAM and DualSPHysics. | 16 |

1 Introduction

Sea dikes and quay walls with horizontal cantilever slabs or storm return walls start to find more and more employ worldwide as coastal defences or berthing structures. A cantilever is a rigid structural element anchored, at only one end, to a vertical support. Vertical structures with cantilever slabs or pier structures are generally used to minimise wave reflection (in case of coastal defences) and/or to reduce wave overtopping. Examples of this type of structures can be found in the European Northern Countries (e.g. Blankenberge pier, in Belgium, or the Brighton Marine Palace and Pier, in U.K.). The design of such structures requires proper assessment of the action exerted by sea waves especially in those areas characterised by wide tidal variation. During storms these structures might be exposed to violent wave impacts especially during high tides. These violent events include waves running up against the vertical part and slamming beneath the horizontal deck (Kisacik, 2012).

Even though plenty of works have been published on the interaction between sea waves and coastal structures over the past decades, there is still a lack of literature about wave impacts on vertical structures with overhanging cantilever slabs. Goda (1974), Kortenhaus *et al.* (1998), Oumeraci *et al.* (2000) and more recently Van Doorslaer *et al.* (2017) - the list is not exhaustive - are just a few remarkable examples, where the authors studied the wave impact on vertical structures to determine the relationship between wave loading and sea wave hydrodynamics. However, most of these studies lack of any analysis on uplift forces exerted on horizontal slabs. This analysis is present in just a few examples like McConnell *et al.* (2003) who investigated the uplift loads below horizontal decks or Douglass *et al.* (2006) who carried out an accurate analysis related to forces on US highway bridges exposed to hurricane waves. More recently, Cuomo *et al.* (2007) developed a prediction method for wave loading. However, there is no general procedure to assess wave loads on vertical structures with overhanging horizontal cantilever slabs. Only a few works present a consistent analysis on this topic. Kisacik (2012) carried out an intensive study on wave impact of regular and irregular waves on a particular geometry that aimed to resemble the Blankenberge pier (Belgium). Kisacik *et al.* (2012) discussed the impact of regular waves on horizontal cantilever slabs focusing on the influence of the breaker type on the wave loads. Further studies on wave impacts on similar structures were conducted at Flanders Hydraulics Research (Suzuki *et al.*, 2015; to provide a first estimation of wave forces on a quay structure supported by piles, located in Oostende harbour. The uplift force was estimated based on conclusions from a physical scale model research on a similar structure (Kisacik *et al.*, 2012). However, this previous analysis was done using a number of simplifications/assumptions, restricting the accuracy/reliability of the force estimation, in particular for the estimation of the uplift forces based on Kisacik *et al.* (2012).

Physical model tests and numerical modelling represent two possible alternatives to more simplified studies, in order to characterize the wave impact forces on pier/cantilever structures. When physical model tests are not feasible or analytical and semi-empirical formulas are not available, numerical modelling offers a useful and complementary tool to assess the effects of sea wave impact on coastal structures (e.g. Altomare *et al.*, 2015a; Didier *et al.*, 2014; Vanneste *et al.*, 2014). The main advantage of numerical modelling is the capability to simulate any scenario with reduced costs. Numerical models are not restricted to a very specific range of application such as semi-empirical equations. Besides, numerical models do not suffer from scale effects and can provide information on physical quantities that could be difficult to measure in a scaled model or in prototype. Traditional Computational Fluid Dynamics (CFD) techniques such as volume-of-fluid methods (VOF) have been used to study wave-structure interaction (Kleefsman *et al.*, 2005; Higuera *et al.*, 2013) and to design breakwaters (Vanneste and Troch, 2012). However, Eulerian numerical methods, such as those based on the finite volume technique, require expensive mesh generation and have severe technical challenges associated with implementing conservative multi-phase schemes that can capture the nonlinearities within rapidly changing geometries. The recent popularity of meshless schemes is due to the fact that they allow overcoming part of the drawbacks that characterize the

mesh-based schemes. Methods such as Smoothed Particle Hydrodynamics (SPH) (Viouleau, 2012), Monte Carlo methods (Geeraerts *et al.*, 2009) and the particle finite element method (PFEM) (Oñate *et al.*, 2011) are examples of mesh-free schemes.

The SPH method was developed originally for astrophysics in the 1970s (Lucy, 1977); since then, SPH has been successfully applied to several fields of engineering and Computational Fluid Dynamics. In SPH the continuum is replaced by particles, which move according to the governing dynamics. Differently from Eulerian methods, no special tracking is used in SPH to detect the free surface. In addition, the domain is multiply-connected due to the Lagrangian nature of the method. As a consequence, large deformations can be efficiently treated since there is no mesh distortion, making SPH an ideal technique to study violent free-surface motion. Thanks to this property, SPH has been used to describe a variety of free-surface flows, including wave propagation over a beach (e.g. Monaghan and Kos, 1999), wave-structure interaction (e.g. Colagrossi and Landrini, 2003), and dam breaks (e.g. Gómez-Gesteira and Dalrymple, 2004). During the last decade SPH has been widely applied to coastal engineering (Gotoh *et al.*, 2004; Shao, 2005; Khayyer *et al.*, 2009; Ren *et al.*, 2014). More recently, St-Germain *et al.* (2014) used SPH to investigate the hydrodynamic forces induced by the impact of rapidly advancing tsunamis, and Altomare *et al.* (2015a) validated the SPH-based DualSPHysics model against experimental data of wave loadings for typical cases from the Belgian coast. Even, the technique is promising for industrial applications (Shadloo *et al.*, 2016).

DualSPHysics (Gómez-Gesteira *et al.*, 2012a, 2012b; Crespo *et al.*, 2015) was conceived to use SPH for real engineering problems. The model is open source and can be freely downloaded from <http://www.dual.sphysics.org>. DualSPHysics includes a software that can be run on either CPUs or GPUs (graphics cards with powerful parallel computing). GPUs offer greater computing power than CPUs, and they are an affordable option to accelerate SPH modelling. Therefore, the simulations conducted in this study were executed using a GPU card installed on a personal computer. The GPU implementation of DualSPHysics has been rigorously validated (Crespo *et al.*, 2011). Further details on the model can be found in Domínguez *et al.* (2011, 2013a, 2013b).

In the present work, DualSPHysics is used to simulate wave impacts on a particular vertical structure with overhanging horizontal cantilever slab. Numerical results will be first compared with experimental data described in Kisacik *et al.* (2012). Experimental data include free-surface elevations and pressure values against the vertical wall of the structure. In addition, the accuracy and efficiency of DualSPHysics will also be compared with a state-of-the-art mesh-based method: IHFOAM (Higuera *et al.*, 2014a; 2014b).

The main goal of this work is to demonstrate the capability and accuracy of the SPH technique to predict the free-surface elevation and the horizontal force exerted by waves on sea walls with horizontal cantilever slab. DualSPHysics will be shown to have achieved the needed maturity to be compared with state-of-the-art Eulerian mesh-based models.

This work was made in collaboration with the Environmental Physics Laboratory (EPHysLab) from Vigo University (Ourense, Spain) and it was partially financed by Xunta de Galicia under project “Programa de Consolidación e Estructuración de Unidades de Investigación Competitivas (Grupos de Referencia Competitiva) GRC2013-001” and under project “NUMANTIA ED431F 2016/004”. The work was also funded by the Ministry of Economy and Competitiveness of the Government of Spain under project “WELCOME ENE2016-75074-C2-1-R”. The experimental data were provided by Dr. Dogan Kisacik (Dokuz Eylül University) and Tom Versluys (Ghent University).

2 Numerical models

2.1 DualSPHysics model

DualSPHysics is a numerical model based on the Smoothed Particle Hydrodynamics (SPH) method. A complete description of DualSPHysics can be found in [Crespo *et al.*, 2015]. SPH is a Lagrangian and mesh-less method where the fluid is discretised into a set of particles that are nodal points where physical quantities (such as position, velocity, density, pressure) are computed as an interpolation of the values of the neighbouring particles. The contribution of these neighbours is weighted using a kernel function (W) that measures that contribution starting from the initial particle spacing. This distance between particles is normalized using the smoothing length (h_{SPH}), which is the characteristic length that defines the area of influence of the kernel. The kernel presents compact support, so that the contribution of particles beyond a cut-off distance (here $2h_{SPH}$) is not considered.

The mathematical fundamental of SPH is based on integral interpolants. Any function F can be computed by the integral approximation.

$$F(\mathbf{r}) = \int F(\mathbf{r}') W(\mathbf{r} - \mathbf{r}', h_{SPH}) d\mathbf{r}' \quad (1)$$

This function F can be expressed in discrete form based on particles. Thus, the approximation of the function is interpolated at particle a and the summation is performed over all the particles within the region of compact support of the kernel:

$$F(\mathbf{r}_a) \approx \sum_b F(\mathbf{r}_b) W(\mathbf{r}_a - \mathbf{r}_b, h_{SPH}) \frac{m_b}{\rho_b} \quad (2)$$

where the volume associated to the neighbouring particle b is m_b/ρ_b , being m and ρ mass and density respectively. The discrete SPH system of equations of a weakly compressible fluid is, according to Monaghan (1992):

$$\left. \begin{aligned} \frac{d\rho_a}{dt} &= \sum_b m_b (\mathbf{v}_a - \mathbf{v}_b + \psi_{ab}) \cdot \nabla_a W_{ab} \\ \frac{d\mathbf{v}_a}{dt} &= - \sum_b m_b \left(\frac{P_b + P_a}{\rho_b \cdot \rho_a} + \Pi_{ab} \right) \nabla_a W_{ab} + \mathbf{g} \\ \frac{d\mathbf{r}_a}{dt} &= \mathbf{v} \end{aligned} \right\} \quad (3)$$

where t is time, r position, v velocity, P pressure, ρ density, m mass, $g = (0, 0, -9.81) \text{ m/s}^2$ the gravitational acceleration and W_{ab} the kernel function that depends on the distance between particles a and b . One option is the Quintic kernel (Wendland, 1995) where the weighting function vanishes for initial particle spacing greater than $2h_{SPH}$. Π_{ab} is the viscous term according to the artificial viscosity proposed in Monaghan (1992). ψ_{ab} is the diffusion term introduced in the so called delta SPH approach proposed by Molteni and Colagrossi (2009).

The system is closed with the Tait's equation of state that allows computing pressure from density values

$$P = B \left[\left(\frac{\rho}{\rho_0} \right)^\gamma - 1 \right] \quad (4)$$

where $\gamma=7$ is the polytropic constant and $B=c_0^2\rho_0/\gamma$, being ρ_0 the reference density and c_0 the numerical speed of sound.

Dynamic Boundary Conditions (DBC) were used following Crespo *et al.* (2007). Waves were generated by means of moving boundaries that mimic the movement of a wavemaker in a physical facility. In the present study, a piston-type wavemaker that moves with a pre-imposed displacement was considered to generate monochromatic and random waves. In addition, an active wave absorption technique was applied to prevent re-reflection at the piston. Details on wave generation and absorption can be found in Altomare *et al.* (2015b).

2.2 IHFOAM

IHFOAM (Higuera *et al.*, 2014a; 2014b) will be considered here for comparison purposes, so only a brief description of the model will be provided. IHFOAM is a mesh-based numerical model that uses the volume of fluid discretization method (VOF) to solve the Reynolds averaged Navier-Stokes (RANS) equations for two incompressible phases (water and air). IHFOAM derives from a more general numerical model named OpenFOAM® by using the solving procedure interFoam included in the latter one. Besides, the code IHFOAM improves the capability of OpenFOAM® for wave generation and active wave absorption by adding new boundary conditions avoiding the definition of moving boundaries. The use of moving boundaries increases the computational time since the mesh has to be redefined every time step. For a more detailed explanation of wave generation and absorption methods, the reader is referred to Higuera *et al.* (2015).

3 Case of study

3.1 The physical model

The physical model tests have been carried out in the wave flume (30 m × 1 m × 1.2 m) of Ghent University (Belgium). The vertical structure with horizontal slab was located 22.5 m away from the wavemaker on a uniform slope, being the depth 0.5 m at the location of the structure. The structure was 0.3 m high and 0.6 m long and it was equipped with 10 sets of pressure sensors. The foreshore slope was 1/20. Eight wave gauges were used to measure the free-surface elevation along the flume and a high speed camera (HSC) to record the development of the wave breaking mechanism. A sampling frequency of 20 kHz was considered for pressure recording while the free-surface elevation was sampled at 40 Hz.

Figure 1 shows a schematic view of the model including the position of the wave gauges and the pressure sensors. A complete set of physical tests was conducted using four different initial water depths and different wave periods. For each combination of water depth and wave period, the wave height was increased in successive tests to achieve the range from non-breaking to broken waves.

In the present study, only two values of water depth at the toe of the structure ($h_s = 0.105$ m and 0.135 m) were considered. Table 1 shows the distance to the resistive wave gauges measured from the wave generator. The position of the pressure sensors located at the vertical wall (distance measured from the toe of the structure), and at the horizontal wall (distance measured from the vertical wall) are shown in Table 2 (see Figure 1).

Figure 1. Setup of the experiment.

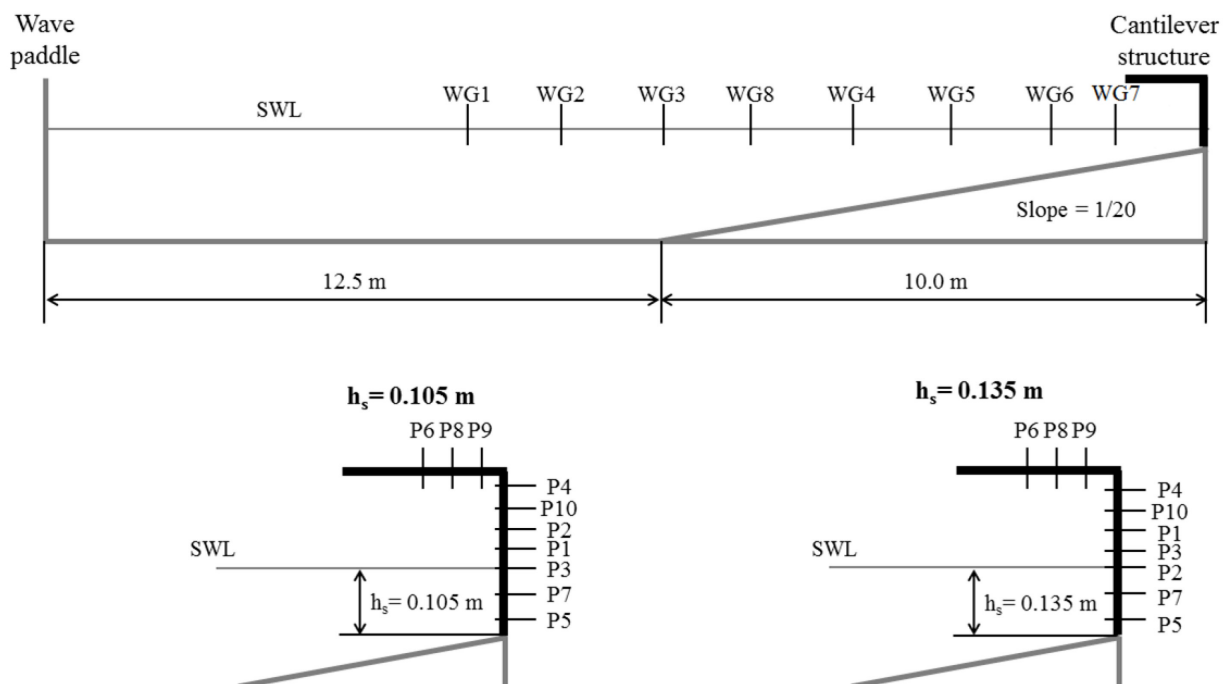


Table 1. Distance (m) to the wave gauges measured from wave paddle.

| WG1 | WG2 | WG3 | WG8 | WG4 | WG5 | WG6 | WG7 |
|-------|-------|------|-------|-------|-------|------|-------|
| 11.32 | 11.81 | 12.5 | 20.59 | 20.86 | 21.25 | 21.5 | 21.85 |

Table 2. Distance (m) from the toe of the structure to the pressure sensors located on the vertical wall and distance from the vertical wall to the pressure sensors located on the horizontal wall (see Figure 1)

| Vertical wall | | | | | | | | Horizontal wall | | | |
|----------------------|-------|-------|-------|-------|-------|-------|-------|-----------------|-------|-------|-------|
| | P5 | P7 | P3 | P1 | P2 | P10 | P4 | | P9 | P8 | P6 |
| $h_s=0.105\text{ m}$ | 0.015 | 0.06 | 0.105 | 0.150 | 0.195 | 0.24 | 0.285 | | 0.010 | 0.040 | 0.085 |
| | | | | | | | | | | | |
| | P5 | P7 | P2 | P3 | P1 | P10 | P4 | | P9 | P8 | P6 |
| $h_s=0.135\text{ m}$ | 0.015 | 0.075 | 0.135 | 0.165 | 0.21 | 0.255 | 0.285 | | 0.010 | 0.040 | 0.085 |

3.2 Wave conditions

In the present study, wave conditions were chosen to be representative of SBW (Slightly Breaking Waves) breaker type (see Kisacik *et al.* (2012) for further definitions on the breaker types). This breaker type, which was first defined by Oumeraci *et al.* (1993) as an incomplete breaking process, results in violent impacts on vertical structures.

Four different wave conditions were used for numerical validation. A regular wave train of only 18 waves was generated to avoid cross-waves due to high reflection. Wave height (H), depth (d) near the piston and depth at the toe of the structure are summarised in Table 3. Wave period (T) was equal to 2.2 s in all cases.

Table 3. Wave conditions

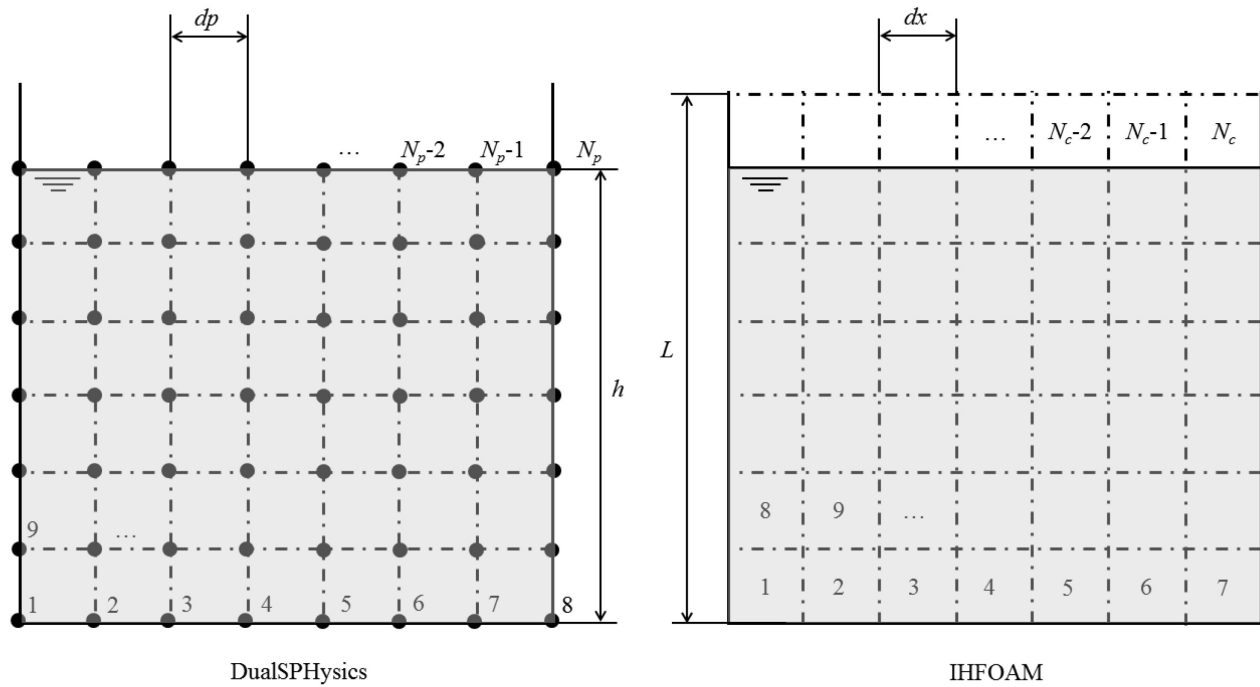
| | H (m) | d (m) | h_s (m) | T (s) |
|--------|---------|---------|-----------|---------|
| Wave#1 | 0.060 | 0.605 | 0.105 | 2.2 |
| Wave#2 | 0.065 | 0.605 | 0.105 | 2.2 |
| Wave#3 | 0.070 | 0.605 | 0.105 | 2.2 |
| Wave#4 | 0.105 | 0.635 | 0.135 | 2.2 |

Waves are generated in a different way in both models. DualSPHysics generates the desired waves of Table 3 by mimicking the wavemaker movement using the time series of the real displacement of the wave generator during the physical tests. By contrast, IHFOAM generates waves starting from the real displacement of the experimental wave generator but without using moving boundaries.

In DualSPHysics, the numerical tank is created with a pre-processing tool that allows creating particles starting from any type of complex geometry. This tool employs a 3-D Cartesian lattice to locate particles. The idea is to build any object using particles. These particles are created at the nodes of the 3-D Cartesian lattice. First, the lattice nodes around the object are defined and then particles are created only at the nodes needed to draw the desired geometry. Only the initial size of the lattice needs to be defined which will be the initial inter-particle spacing (dp). In this work, an initial inter-particle spacing of 0.003 m was defined leading to approximately 1.3 M fluid particles. Since IHFOAM is a meshbased method, the numerical domain needs to be initially meshed by using, for example, the blockMesh function. The defined mesh will be a set of cells with a characteristic cell size (dx) of 0.003 m. This leads to a mesh with 1.2 M quadrilateral cells. A physical time of 70 s was simulated by both models and a sampling frequency of 100 Hz was used both for the pressure and free-surface elevation. The sampling frequency in experiments was resampled according to the numerical one.

Figure 2 shows an example of the discretization of a square box of size L with a water depth equal to h using DualSPHysics and IHFOAM. The initial particle spacing defined with DualSPHysics is equal to dp leading to N_p particles of water and the characteristic size of the mesh cells of IHFOAM is equal to dx leading to N_c cells of water and a few of the air phase. In this case, dp is equal to dx while N_p is slightly higher than N_c , although similar.

Figure 2. Discretization of a square domain of size $L \times h$ using DualSPHysics and IHFOAM where $dp=dx$ and $N_p \approx N_c$.



The efficiency and the computational cost of DualSPHysics and IHFOAM will be compared later. For this purpose, different resolutions in the numerical models will be analysed. Both models will be executed using an initial distribution with a spacing (dp or dx) of 0.003, 0.006 and 0.009 m.

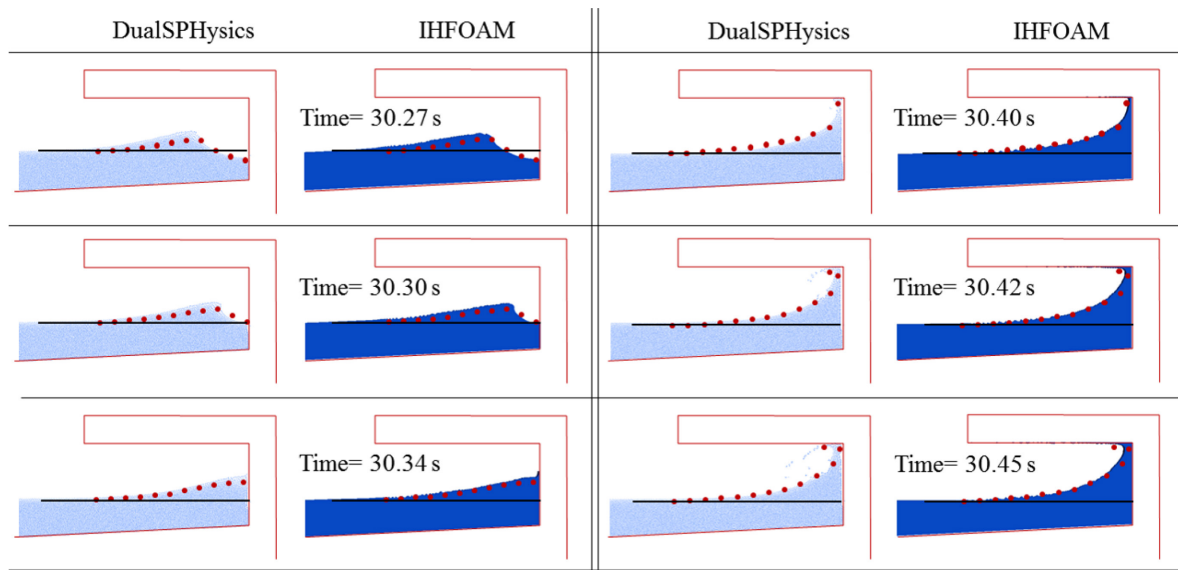
4 Results and discussion

This section shows the numerical results obtained using DualSPHysics compared with the experimental data from the physical tests and with the numerical results obtained using IHFOAM. The measurements during the physical tests consist of free-surface elevation and pressures caused by monochromatic (i.e. regular) waves on the vertical part of the scale model. The development of waves, such as the wave shape at the moment of the impact, was also recorded using a high-speed camera system. During next sections (4.1 to 4.3) the resolution of 3 mm ($\Delta p = \Delta x = 0.003$ m; high resolution) will be used in both numerical models. During the experimental campaign, a sampling frequency of 20 kHz was used for pressure recording while the free-surface elevation was sampled at 40 Hz. The total duration of the numerical wave equal to 70 s of real physical time; the numerical data were acquired at 100 Hz. Only in section 4.4, different resolutions are used for comparison purposes.

4.1 Wave shape development

A visual comparison of the wave shape development for the SBW breaker type obtained from simulations and from experimental tests for Wave#2 is shown in Figure 3. Black line represents the still water level (SWL) and red dots represent the experimental free-surface profile observed in the physical tests (from Kisacik *et al.*, 2012). The three instants immediately before the collision ($t=30.27$ s, 30.30 s and 30.34 s) show a good agreement between the physical model test and both numerical models. The impact on the top of the structure takes place at $t=30.40$ s and is properly reproduced by both models. After the impact ($t=30.42$ s, and 30.45 s) the fluid in DualSPHysics splashes back and propagates downwards while the water phase in IHFOAM goes backwards and remains stuck to the horizontal part of the structure. These differences are related to the different approaches to define the boundary conditions in both numerical models and to the existence of air phase in IHFOAM model, which is not being considered in DualSPHysics. Experimental results show an intermediate behaviour after the impact since part of the water is stuck to the horizontal roof and part of the water splashes back. Hence, it can be concluded that DualSPHysics and IHFOAM reproduce the wave propagation and the impact observed in the physical tests with a similar reliability. After the impact on the horizontal part of the structure both numerical models show a deviation from the experimental tests.

Figure 3. Different instants of the DualSPHysics and IHFOAM simulations of Wave#2 compared with the experimental wave profiles (red dots).



4.2 Free-surface elevation

The time series of the free-surface elevation (η) for the first and the last wave gauges (WG1 and WG7 in Table 1) obtained with DualSPHysics and IHFOAM for Wave#2 are shown in Figure 4. The experimental data are also included for visual comparison. The numerical results resemble the physical ones in terms of free surface elevation in both wave gauges. Only some discrepancies appear in WG1 over the last 15 s due to the interaction of incident with reflected waves since wave absorption is carried out in a different way in both numerical models.

The time series of the free-surface elevations obtained in the rest of the cases (other wave gauges and other wave conditions) show a similar agreement. Besides the visual comparison, the accuracy of the numerical results for the free-surface elevation with the experimental results is represented using Taylor's diagrams (Taylor, 2001) for all the cases. The agreement between numerical and experimental results is quantified in terms of their correlation, centred root-mean-square difference (RMS) and standard deviation (normalized). Thus, Figure 5 shows the Taylor's diagrams of the four wave conditions. The experimental free-surface elevation is used here as reference (Ref) and the coloured dots at each panel of the figure refer to the wave gauge number (according to Table 1) for DualSPHysics (red) and IHFOAM (blue). Correlation coefficients range from 0.7 to 0.97, RMS differences are less than 1.4 and the standard deviations are less than 1.0 in all cases. This proves the good accuracy of both numerical models when comparing with the physical tests. It can also be observed that DualSPHysics slightly outperforms IHFOAM for Wave#1, Wave#2 and Wave#4, whilst IHFOAM outperforms DualSPHysics for Wave#3.

Figure 4. Time series of numerical (DualSPHysics and IHFOAM) and experimental free-surface elevation for Wave#2 case at WG1 and WG7

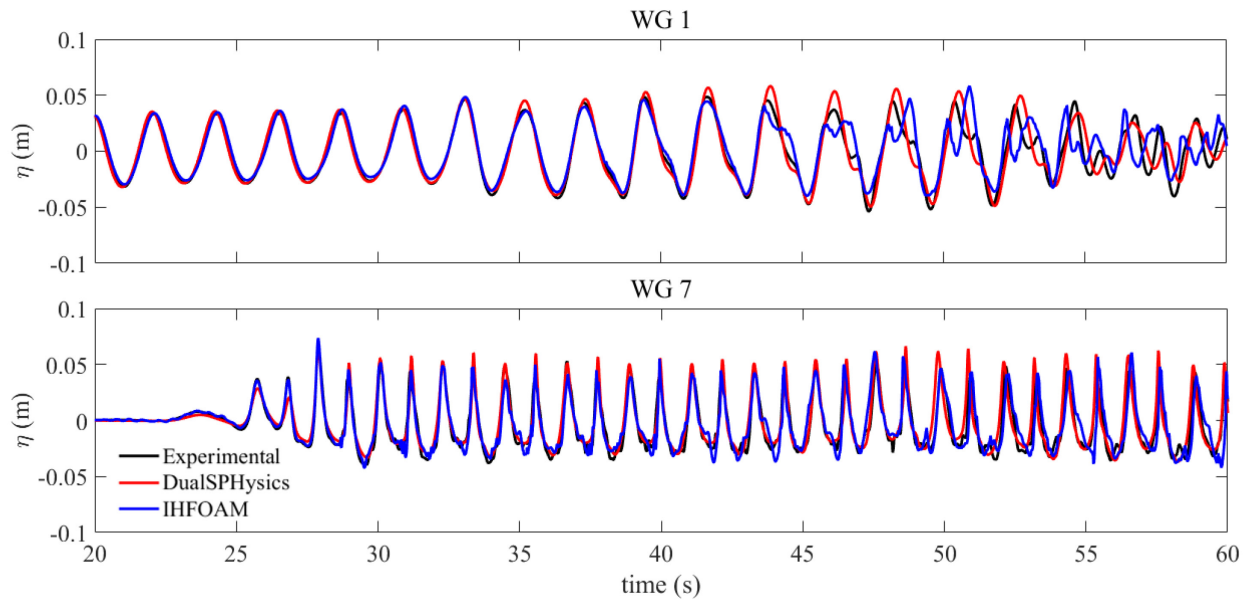
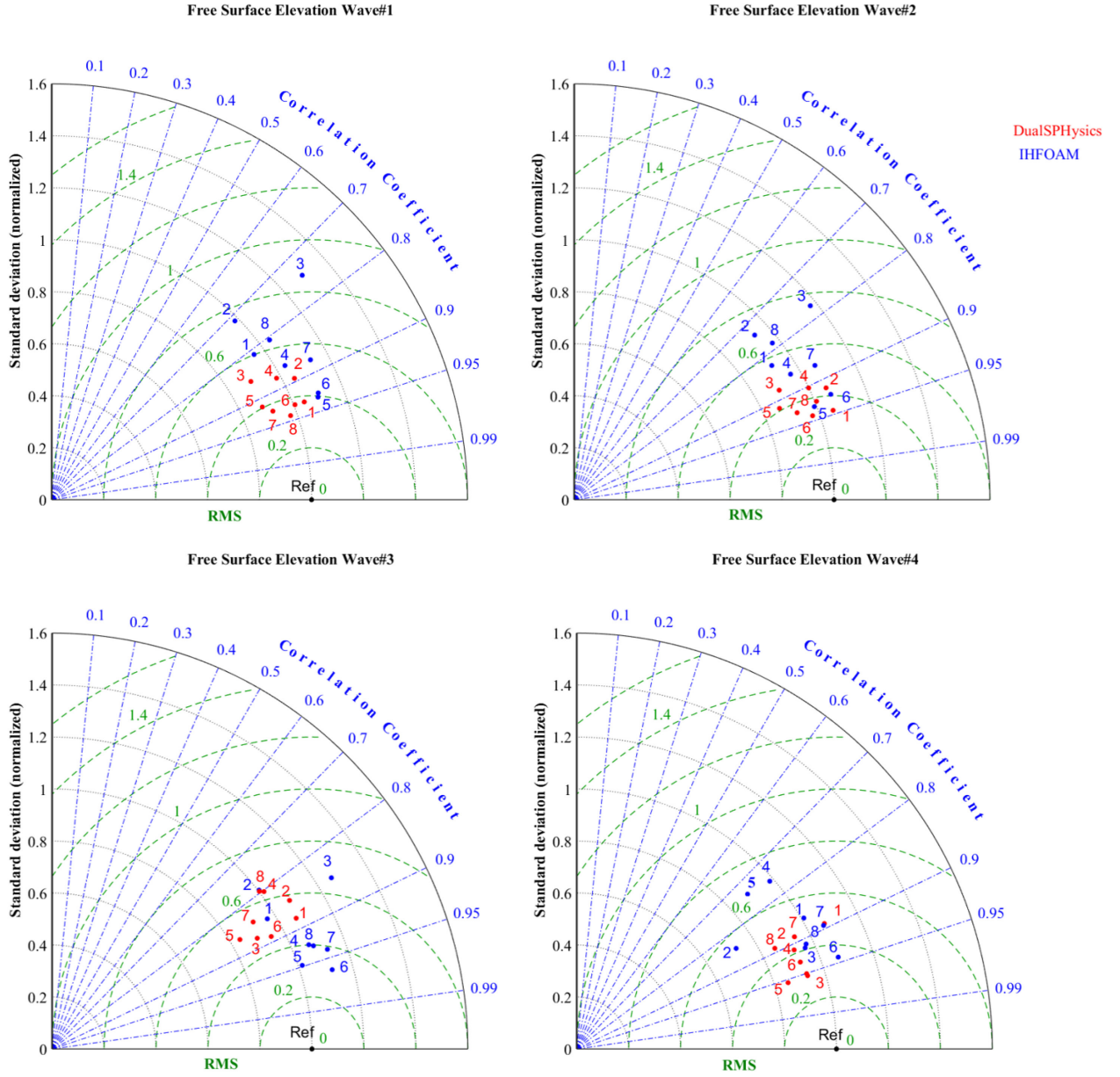


Figure 5. Taylor's diagrams with comparison of numerical free-surface elevations for DualSPHysics (red numbers) and IHFOAM (blue numbers) using the experimental free-surface elevation as reference (Ref).



An additional approach to analyse the reliability of the two numerical models to reproduce the free-surface elevation is the computation of the skill index S . According to Taylor (2001) this index can be defined as:

$$S = \frac{4(1+R)^4}{\left(\sigma_f + \frac{1}{\sigma_f}\right)^2 (1+R_0)^4} \quad (5)$$

where R is the correlation factor, σ_f is the standard deviation of the numerical data, and R_0 is the maximum correlation attainable for the model (equal to 1 in this case). The index S can range from 0, in the case of models with no skill to reproduce the experimental observations, to 1, for models with a high skill to reproduce the experiments. Table 4 shows the values of the skill index S for each wave gauge (S_{eta}) and the four wave conditions. It can be observed that the values of the skill index obtained with DualSPHysics are

closer to 1 than obtained with IHFOAM for Wave#1, Wave#2 and Wave#4 while the opposite is observed for Wave#3. This is also depicted in the last two rows where the mean skill index is higher for DualSPHysics in three of the four cases and the standard deviation is always lower for DualSPHysics. Thus, we can affirm that for the cases under study and for this particular high spatial resolution DualSPHysics slightly outperforms IHFOAM.

Table 4. Skill index calculated for wave elevation at 8 gauges. Mean and standard deviation of the skill index was also calculated using the value of the index at every gauge for every wave (last two rows).

| | Wave #1 | | Wave #2 | | Wave #3 | | Wave #4 | |
|------|---------|--------|---------|--------|---------|--------|---------|--------|
| | DualSPH | IHFOAM | DualSPH | IHFOAM | DualSPH | IHFOAM | DualSPH | IHFOAM |
| WG1 | 0.87 | 0.67 | 0.89 | 0.69 | 0.78 | 0.74 | 0.80 | 0.76 |
| WG2 | 0.80 | 0.54 | 0.84 | 0.57 | 0.72 | 0.65 | 0.83 | 0.66 |
| WG3 | 0.74 | 0.54 | 0.77 | 0.60 | 0.77 | 0.70 | 0.90 | 0.84 |
| WG8 | 0.89 | 0.66 | 0.86 | 0.63 | 0.66 | 0.86 | 0.78 | 0.80 |
| WG4 | 0.78 | 0.76 | 0.82 | 0.76 | 0.65 | 0.86 | 0.86 | 0.59 |
| WG5 | 0.83 | 0.86 | 0.82 | 0.87 | 0.73 | 0.90 | 0.89 | 0.57 |
| WG6 | 0.87 | 0.86 | 0.89 | 0.85 | 0.79 | 0.91 | 0.90 | 0.89 |
| WG7 | 0.86 | 0.77 | 0.86 | 0.77 | 0.72 | 0.87 | 0.79 | 0.83 |
| mean | 0.83 | 0.71 | 0.84 | 0.72 | 0.72 | 0.81 | 0.84 | 0.74 |
| std | 0.05 | 0.12 | 0.04 | 0.11 | 0.05 | 0.10 | 0.05 | 0.12 |

4.3 Wave forces onto vertical wall

The force exerted onto the vertical wall was also computed for both numerical models and compared with experimental results. However, the procedure to obtain the force values are different for the three solutions. On one hand, the forces obtained from physical tests and those obtained with IHFOAM use the values of the pressure gauges (Kisacik *et al.*, 2012). On the other hand, numerical forces obtained with DualSPHysics are directly computed starting from the acceleration values of the boundary particles of the vertical wall, so that, the force will be the summation of those accelerations multiplied by the mass of each boundary particle of the wall (as shown in Altomare *et al.*, 2015a).

Figure 6 shows the time series of numerical (DualSPHysics and IHFOAM) and experimental horizontal force onto the vertical wall of the structure for Wave#2. Macroscopically, there is a good agreement between experimental and numerical signals. Unexpectedly, the plateau between consecutive peaks is very similar in both numerical simulations and slightly different from the experiments. In both numerical models the force decreases continuously until values close to zero, which is not observed in the experiments. A possible reason for this discrepancy is the quality of the pressure sensors used during the experimental campaign. Quartz high-pressure sensors from Kistler were implemented (see Kisacik *et al.*, 2012). This kind of pressure sensor is especially suited for dynamic pressure measurement. Actually, measurements have shown the good performance of these pressure sensors for impulsive loading and violent impacts. However, sensors show a downward drift or decay in the signal after the impact, when only hydrostatic pressure or just to the air pressure act on the sensor. This decay was corrected during post-processing for a proper analysis of the results, which can bias the experimental results. Therefore, the part of the plateau is less reliable in

experiments and can result in an apparent lack of reliability in numerical models when, in fact, those numerical results are more accurate than the experimental ones for that zone. Finally, it is worth mentioning the non-repeatability of the peaks in the time force series in the physical tests. In fact, the wave impacts vary significantly during each individual test, even though the generated waves are nominally identical (Kisacik *et al.*, 2012). This non-repeatability is a known phenomenon in physical tests (e.g. Peregrine, 2003; Bullock *et al.*, 2007 and Kisacik *et al.*, 2012) and makes more difficult to analyse the accuracy of forces than previously done for water elevation.

Figure 6. Time series of the numerical (DualSPHysics and IHFOAM) and experimental horizontal force exerted against the vertical wall of the structure for Wave#2.

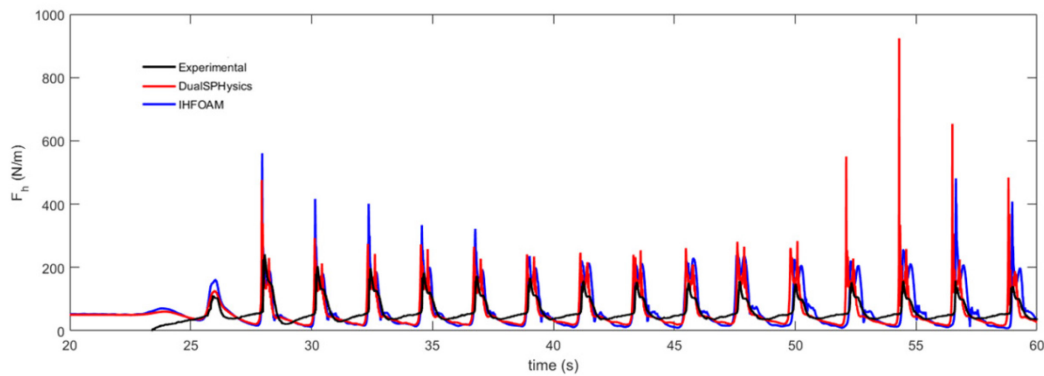
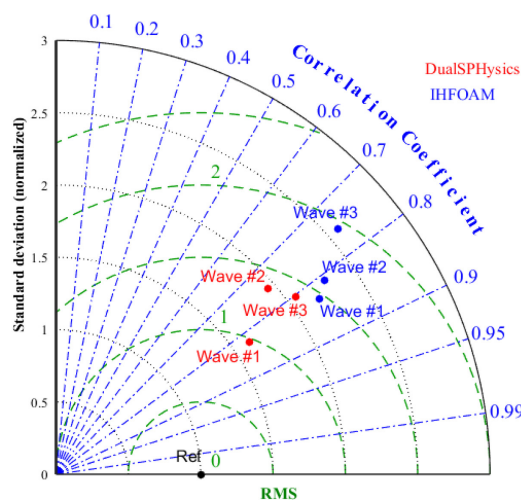


Figure 7 shows the accuracy of numerical horizontal forces compared with experimental data using Taylor's diagrams (Taylor, 2001) for Wave#1, Wave#2 and Wave#3 (experimental forces for Wave#4 were not provided). The correlation coefficients are similar for both models, although for DualSPHysics RMS is closer to 0 and standard deviation is closer to 1, which results a slightly better performance when compared to IHFOAM.

Figure 7. Taylor diagram with comparison of numerical horizontal force for DualSPHysics (red) and IHFOAM (blue) using the experimental free-surface elevation as reference (Ref).



The skill index S defined in Eq. (5) was also computed for the horizontal force. Table 5 shows the value of this index obtained for Wave#1, Wave#2 and Wave#3. It can also be observed that slightly higher values are achieved using DualSPHysics.

Table 5. Skill index for the horizontal force of DualSPHysics and IHFOAM models.

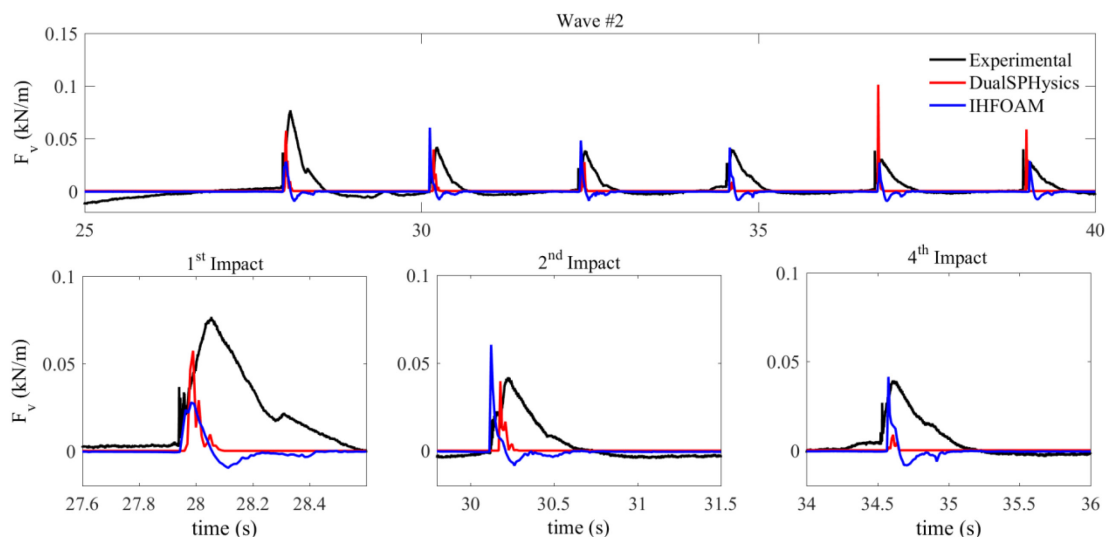
| | <i>DualSPHysics</i> | <i>IHFOAM</i> |
|--------|---------------------|---------------|
| Wave#1 | 0.55 | 0.40 |
| Wave#2 | 0.39 | 0.36 |
| Wave#3 | 0.41 | 0.27 |
| mean | 0.45 | 0.34 |
| std | 0.09 | 0.07 |

4.4 Uplift wave forces

The uplift forces exerted onto the horizontal slab were computed for both numerical models and compared with experimental results only for Wave#2. Figure 8 shows the time series of numerical (DualSPHysics and IHFOAM) and experimental uplift forces onto the horizontal slab.

In contrast with horizontal forces shown in previous paragraphs, numerical uplift forces exhibit a clear deviation from experimental results. Both numerical models show different behaviour for each impact from experimental results. Again, the possible reason for this discrepancy is the quality of the pressure sensors used during the experimental campaign and the correction of the downward drift. One could argue that the lack of the air-phase in DualSPHysics might cause inaccuracies especially for the uplift forces that, in the studied case, are caused by highly aerated overturning flows. But this might be in contrast with IHFOAM, that does include the air phase and yet shows significant differences with the physical model tests. If the peak values, for some events, can be comparable, yet the impulse of each impact is different: both numerical models are characterized by quite sharp rise phase and short duration time, whereas the physical model results show less impulsive events.

Figure 8. Time series of the numerical (DualSPHysics and IHFOAM) and experimental uplift forces exerted against the horizontal slab for Wave#2.

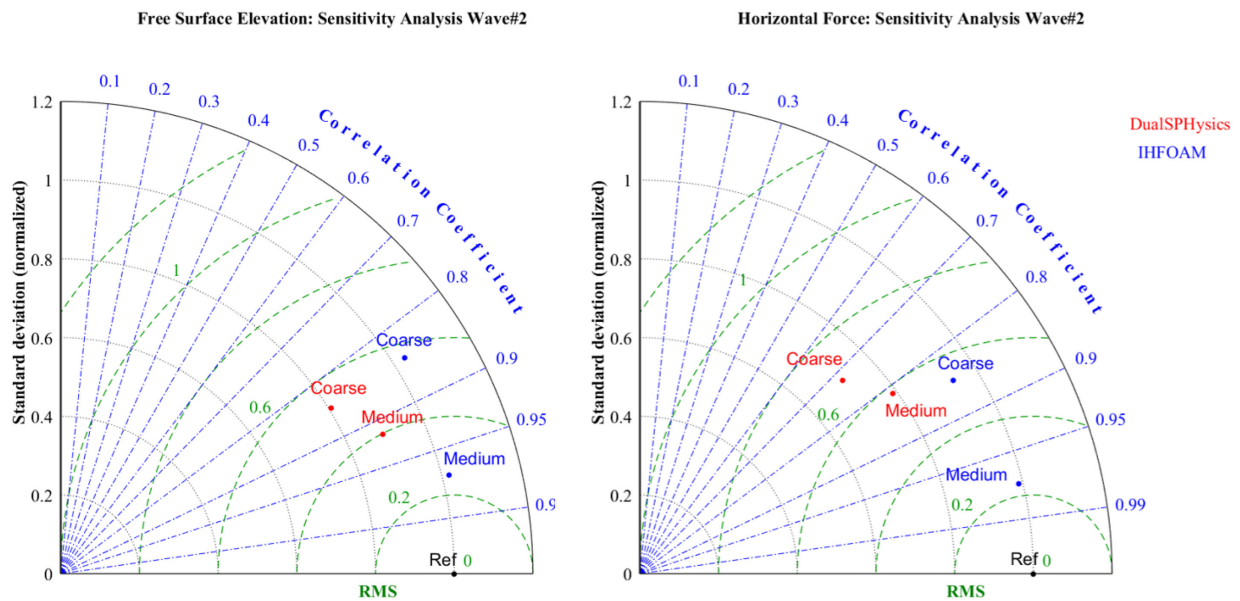


4.5 Sensitivity analysis of the numerical models to spatial resolution

In order to obtain the sensitivity of the numerical models to spatial resolution, Wave#2 was simulated for different values of dp (or dx). Fine resolution (0.003 m as used in previous section), medium resolution (0.006 m) and coarse resolution (0.009 m). This classification was carried out in terms of the ratio wave amplitude dp (or dx). This ratio ranges from approximately 22 for high resolution to only 7 for low resolution.

Figure 9 shows the Taylor's diagrams obtained for free-surface elevation at WG7 (the wave gauge closest to the structure) and the horizontal force onto the vertical wall of the structure using the three resolutions. Fine resolution was used as reference (Ref) to analyse how accuracy is lost when decreasing resolution. In general, the accuracy of both numerical models decreases with resolution as expected. However, the standard deviation of IHFOAM is closer to 1 and the RMS is lower, which suggests that the loss of resolution has less impact on accuracy for IHFOAM. This means that IHFOAM can reproduce the experimental observations with a good accuracy for the different resolutions, whilst DualSPHysics requires a higher spatial resolution.

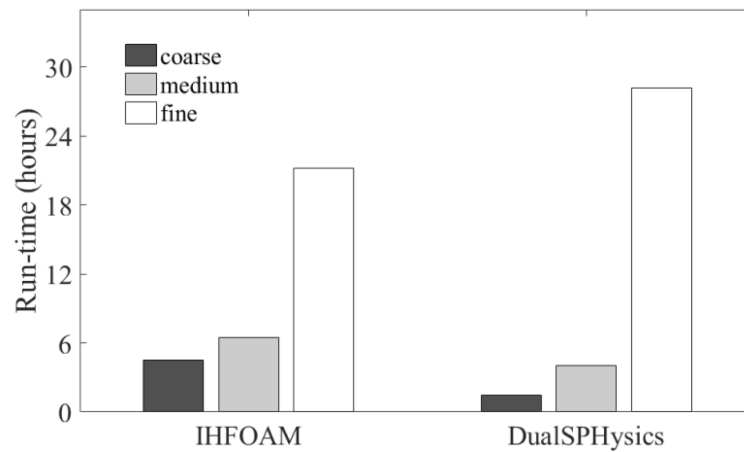
Figure 9. Taylor diagram with sensitivity analysis to resolution of free-surface elevation at WG7 (left panel) and horizontal force onto the vertical wall (right panel) with DualSPHysics and IHFOAM for Wave #2.



4.6 Model efficiency

Finally, the efficiency of both numerical codes was analysed for Wave#2. This comparison is not straightforward due to the peculiarities of both models. From a computational point of view, IHFOAM is designed to run on multicore CPUs while DualSPHysics is especially well suited to run on GPUs. Here, we have run IHFOAM on an Intel Xeon E5-2640 (using 16 physical cores) and DualSPHysics simulations on a GPU card NVIDIA Titan Black. Three different resolutions were considered as in previous subsection (0.003, 0.006 and 0.009 m) being the number of particles similar to the number of cells. Figure 10 shows the run-time (in hours) for the different models and spatial resolutions.

Figure 10. Computational times for the different simulations using IHFOAM and DualSPHysics.



Apparently, the performance of both models is similar. DualSPHysics is slightly faster for low and medium resolution but slower for high resolution. However, this comparison is not straightforward as we mentioned above. On the one hand, IHFOAM considers two phases (air and water) and DualSPHysics only one. The use of two phases can result in an unnecessary burden, especially for those cases like the one under study where the entrapped air does not play an important role, while it can be crucial in other cases. On the other hand, the comparison was carried out assuming a regular mesh (the same separation among all nodes). It is a well-known fact that mesh-based models can easily work with adaptive meshes, where the spatial resolution is higher in the areas of interest, near the structure in this case, and lower in the propagation zone. Important advances on this topic have also been carried out for meshless methods over the last few years (Vacondio *et al.*, 2013, Barcarolo *et al.*, 2014), which suggests that the use of an adaptive spatial resolution can also provide an important speed-up in meshless codes. To sum up and despite the difficulty of comparing models of such a different nature, the numerical performance of both models can be considered quite similar.

5 Conclusions

The accuracy and performance of the meshless model DualSPHysics has been assessed for a case that involves violent collisions between sea waves and coastal structures. The particular structural layout consists of a vertical sea wall with a hanging horizontal cantilever slab. Physical model tests of monochromatic waves have been used for comparison purposes. Both water surface elevation and forces were considered. In addition, the accuracy and efficiency of DualSPHysics were compared with results from a state-of-the art mesh-based (IHFOAM) to test the degree of maturity of meshless models.

The main conclusions of the study can be summarized as follows:

- Macroscopically, DualSPHysics is able to reproduce properly the main features of the collision with the coastal structure. Entrapped air does not play a key role in this collision process.
- Both models provide a similar level of accuracy when considering fine spatial resolution for water elevation and horizontal forces. Accuracy is higher for water elevation than for forces, due to the difficulty to measure forces properly in experiments. Overall, DualSPHysics slightly outperforms IHFOAM for both variables.
- However, the accuracy of DualSPHysics decreases faster with resolution. IHFOAM is more stable and performs better at lower resolutions.
- Numerical results from both models of uplift forces diverge from the physical ones. The reasons for this difference might lie in the quality of the pressure sensors employed during the experimental campaign and it would require further investigation.
- Both models show a similar performance, although the comparison is rather qualitative due to the particular features of every model.

In summary, the present work demonstrated that for problems involving violent impact on coastal structures mesh-free methods have achieved the required level of maturity in comparison with mesh-based methods. Mesh-based models like IHFOAM can easily include two phases and are efficient and robust even for low spatial resolution; in addition, the model also allows using variable spatial resolution at each node in a natural way. Models based on SPH technique like DualSPHysics are less efficient when dealing with variable resolution and multiphase problems with very different densities for both phases (water and air for example). Nevertheless, they are especially well suited when dealing with rapidly moving boundaries or floating and moored objects. The combined use of both kind of models is then advisable to overcome the limitations inherent to each approach and take advantage of their strengths.

References

- Altomare, C.; Crespo, A.J.C.; Domínguez, J.M.; Gómez-Gesteira, M.; Suzuki, T. and Verwaest, T. (2015a).** Applicability of Smoothed Particle Hydrodynamics for estimation of sea wave impact on coastal structures. *Coastal Engineering*, 2015a, vol. 96, pp. 1-12.
- Altomare, C.; Suzuki, T.; Domínguez, J.M.; Barreiro, A.; Crespo, A.J.C. and Gómez-Gesteira, M. (2015b).** Numerical wave dynamics using Lagrangian approach: wave generation and passive & active wave absorption. 10th International SPHERIC workshop, 2015b, pp. 216-223.
- Barcarolo, D.A.; Le Touzé, D.; Oger, G.; De Vuyst, F. (2014).** Adaptive particle refinement and derefinement applied to the smoothed particle hydrodynamics method. *Journal of Computational Physics*, vol. 273, pp. 640-657.
- Barreiro, A.; Crespo, A.J.C.; Domínguez, J.M.; Gómez-Gesteira, M. (2013).** Smoothed particle hydrodynamics applied in fluid structure interactions. *WIT Transactions on the Built Environment*, vol. 129, pp. 75-83.
- Bullock, G.N.; Obhrai, C.; Peregrine, D.H.; Bredmose, H. (2007)** Violent breaking wave impacts. Part 1: Results from large-scale regular wave tests on vertical and sloping walls. *Coastal Engineering*, vol. 54(8), pp. 602-617.
- Colagrossi, A.; Landrini, M. (2003).** Numerical simulation of interfacial flows by smoothed particle hydrodynamics. *Journal of Computational Physics*, vol. 191 (2), pp. 448-475.
- Crespo, A.J.C.; Gómez-Gesteira, M.; Dalrymple, R.A. (2007).** Boundary conditions generated by dynamic particles in SPH methods. *Computers, Materials and Continua*, vol. 5(3), pp. 173-184.
- Crespo, A.J.C.; Domínguez, J.M.; Barreiro, A.; Gómez-Gesteira, M.; Rogers, B.D. (2011).** GPUs, a new tool of acceleration in CFD: Efficiency and reliability on smoothed particle hydrodynamics methods. *PLoS ONE*, vol. 6 (6), art. no. e20685.
- Crespo, A.J.C.; Domínguez, J.M.; Rogers, B.D.; Gómez-Gesteira, M.; Longshaw, S.; Canelas, R.; Vacondio, R.; Barreiro, A. and García-Feal, O. (2015).** DualSPHysics: open-source parallel CFD solver on Smoothed Particle Hydrodynamics (SPH). *Computer Physics Communications*, vol. 187, pp. 204-216.
- Cuomo, G.; Tirindelli, M.; Allsop N.W.H. (2007).** Wave-in-deck loads on Exposed Jetties. *Coastal Engineering*, vol. 54(9), pp. 657-679.
- Domínguez, J.M.; Crespo, A.J.C.; Gómez-Gesteira, M.; Marongiu, J.C. (2011).** Neighbour lists in smoothed particle hydrodynamics. *International Journal for Numerical Methods in Fluids*, vol. 67 (12), pp. 2026-2042.
- Domínguez, J.M.; Crespo, A.J.C.; Valdez-Balderas, D.; Rogers, B.D.; Gómez-Gesteira, M. (2013a).** New multi-GPU implementation for smoothed particle hydrodynamics on heterogeneous clusters. *Computer Physics Communications*, vol. 184 (8), pp. 1848-1860.
- Domínguez, J.M.; Crespo, A.J.C.; Gómez-Gesteira, M. (2013b).** Optimization strategies for CPU and GPU implementations of a smoothed particle hydrodynamics method. *Computer Physics Communications*, vol. 184 (3), pp. 617-627.
- Douglass, S.L.; Chen Q. and Olsen J.M. (2006).** Wave forces on bridge decks. Coastal Transportation Engineering Research and Education Center, University of Alabama.
- Geeraerts, J.; Kortenhaus, A.; González-Escrivá, J.A.; De Rouck, J.; Troch, P. (2009).** Effects of new variables on the overtopping discharge at steep rubble mound breakwaters - The Zeebrugge case. *Coastal Engineering*, vol. 56 (2), pp. 141-153.

- Goda, Y.** (1974). The fourth order approximation to the pressure of standing waves. Coastal Eng. In Japan, vol. 10, pp.1-11
- Gómez-Gesteira, M.; Dalrymple, R.A.** (2004). Using a three-dimensional smoothed particle hydrodynamics method for wave impact on a tall structure”, Journal of Waterway, Port, Coastal and Ocean Engineering, vol. 130 (2), pp. 63-69.
- Gomez-Gesteira, M.; Rogers, B.D.; Crespo, A.J.C.; Dalrymple, R.A.; Narayanaswamy, M.; Dominguez, J.M.** (2012). SPHysics - development of a free-surface fluid solver - Part 1: Theory and formulations. Computers and Geosciences, vol. 48, pp. 289-299.
- Gomez-Gesteira, M.; Crespo, A.J.C.; Rogers, B.D.; Dalrymple, R.A.; Dominguez, J.M.; Barreiro, A.** (2012). SPHysics - development of a free-surface fluid solver - Part 2: Efficiency and test cases. Computers and Geosciences, vol. 48, pp. 300-307.
- Gotoh, H.; Shao, S.; Memita, T.** (2004). SPH-LES model for numerical investigation of wave interaction with partially immersed breakwater. Coastal Engineering Journal, vol. 46 (1), pp. 39-63.
- Higuera, P.; Lara, J.L.; Losada, I.J.** (2013). Realistic wave generation and active wave absorption for Navier–Stokes models: application to OpenFOAM®. Coast. Eng., vol. 71, pp. 102–118.
- Higuera, P.; Lara, J.L.; Losada, I.J.** (2014a). Three-dimensional interaction of waves and porous coastal structures using OpenFOAM®. Part I: Formulation and validation. Coastal Engineering, vol. 83, pp. 243-258.
- Higuera, P.; Lara, J.L.; Losada, I.J.** (2014b). Three-dimensional interaction of waves and porous coastal structures using OpenFOAM®. Part II: Application. Coastal Engineering, vol. 83, pp. 259-270.
- Higuera, P.; Losada, I.J.; Lara, J.L.** (2015). Three-dimensional numerical wave generation with moving boundaries. Coastal Engineering, vol. 101, pp. 35-47.
- Khayyer, A.; Gotoh, H.; Shao, S.** (2009). Enhanced predictions of wave impact pressure by improved incompressible SPH methods. Applied Ocean Research, vol. 31 (2), pp. 111-131.
- Kisacik, D.** (2012). Loading Conditions Due to Violent Wave Impacts on Coastal Structures with Cantilever Surfaces. Ghent University, Belgium.
- Kisacik, D.; Troch, P.; Bogaert, P.V.** (2012). Description of loading conditions due to violent wave impacts on a vertical structure with an overhanging horizontal cantilever slab. Coastal Engineering, vol. 60, pp. 201-216.
- Kleefsman, K.M.T.; Fekken, G.; Veldman, A.E.P.; Iwanowski, B.; Buchner, B.** (2005). A Volume-of-Fluid based simulation method for wave impact problems. Journal of Computational Physics , vol. 206 (1), pp. 363-393.
- Kortenhaus, A.; Oumeraci, H.** (1998). Classification of wave loading on monolithic coastal structures. Proceedings of the Coastal Engineering Conference, 1, pp. 867-880.
- Lucy, L. B.** (1977). Astron. J. 82:1013
- Marongiu, J.-C.; Leboeuf, F.; Caro, J.; Parkinson, E.** (2010). Free surface flows simulations in Pelton turbines using an hybrid SPH-ALE method. Journal of Hydraulic Research, vol. 48 (SUPPL. 1), pp. 40-49.
- McConnel, K.J.; Allsop, N.W.H.; Cuomo, G. and Cruickshank, I.C.** (2003). New guidance for wave forces on jetties in exposed locations. COPEDEC VI, Colombo, Sri Lanka.
- Molteni, D.; Colagrossi, A.** 2009. A simple procedure to improve the pressure evaluation in hydrodynamic context using the SPH. Computer Physics Communications, vol. 180(6), pp. 861-872.
- Monaghan, J.J.** (1992). Smoothed particle hydrodynamics. Annual Review of Astronomy and Astrophysics, vol. 30. pp. 543-574.

- Monaghan, J.J.** (1994). Simulating Free Surface Flows with SPH. *Journal of Computational Physics*, vol. 110 (2), pp. 399-406.
- Oñate, E.; Celigueta, M.A.; Idelsohn, S.R.; Salazar, F.; Suárez, B.** (2011). Possibilities of the particle finite element method for fluid-soil-structure interaction problems. *Computational Mechanics*, vol. 48 (3), pp. 307-318.
- Oumeraci, H.; Klammer, P.; Partenscky, H.W.** (1993). Classification of breaking wave loads on vertical structures. *Journal of Waterway, Port, Coastal and Ocean Engineering*, vol. 119 (4), pp. 381-397.
- Oumeraci, H.; Kortenhaus, A.; Allsop, N.W.H.; DeGroot, M.B.; Crouch, R.S.; Vrijling, J.K.; Koortman, H.G.** (2000). *Probabilistic Design Tools for Vertical Breakwaters*. Rotterdam, The Netherlands: Balkema, 392.
- Peregrine, D.H.** (2003). Water-wave impact on walls. *Annual Review of Fluid Mechanics*, vol. 35, pp. 23-43.
- Ren, B.; Wen, H.; Dong, P.; Wang, Y.** (2014). Numerical simulation of wave interaction with porous structures using an improved smoothed particle hydrodynamic method *Coastal Engineering*, vol. 88, pp. 88-100.
- Shadloo, M.S.; Oger, G.; Le Touzé, D.** (2016). Smoothed particle hydrodynamics method for fluid flows, towards industrial applications: Motivations, current state, and challenges. *Computers & Fluids*, vol. 136, pp. 11-34.
- Shao, S.** (2005). SPH simulation of solitary wave interaction with a curtain-type breakwater, *Journal of Hydraulic Research*, vol. 43 (4), pp. 366-375.
- St-Germain, P.; Nistor, I.; Townsend, R.; Shibayama, T.** (2014). Smoothed-particle hydrodynamics numerical modeling of structures impacted by tsunami bores, *Journal of Waterway, Port, Coastal and Ocean Engineering*, vol. 140 (1), pp. 66-81.
- Suzuki, T.; Vanneste, D.; Verwaest, T.; Mostaert, F.** (2015). Force estimation on a quay structure in Ostend: A quick estimation of uplifting force acting on a horizontal plate. Version 4.0. WL Adviezen, 15_085_2. Flanders Hydraulics Research: Antwerp, Belgium.
- Taylor, K.E.** (2001). Summarizing multiple aspects of model performance in a single diagram. *Journal of Geophysical Research*, vol. 106, pp. 7183-7192.
- Vacondio, R.; Rogers, B.; Stansby, P.; Mignosa, P.; Feldman, J.** (2013). Variable resolution for SPH: A dynamic particle coalescing and splitting scheme. *Computer Methods in Applied Mechanics and Engineering*, vol. 256(0), pp. 132 – 148.
- Van Doorslaer, K.; Romano, A.; De Rouck, J.; Kortenhaus, A.** (2017). Impacts on a storm wall caused by non-breaking waves overtopping a smooth dike slope. *Coastal Engineering*, vol. 120, pp. 93-111.
- Vanneste, D.; Troch, P.** (2012). An improved calculation model for the wave-induced pore pressure distribution in a rubble-mound breakwater core. *Coastal Engineering*, vol. 66, pp. 8-23.
- Vanneste, D.; Suzuki, T.; Verwaest, T.; Mostaert, F.** (2015). Force estimation on a quay structure in Ostend: Horizontal force estimation on support pile. Version 4.0. WL Adviezen, 15_085_1. Flanders Hydraulics Research, Antwerp, Belgium.
- Violeau, D.** (2012). *Fluid Mechanics and the SPH Method: Theory and Applications*. Oxford University Press.
- Wendland, H.** (1995). Piecewise polynomial, positive definite and compactly supported radial functions of minimal degree. *Advances in Computational Mathematics*, vol. 4(1), pp. 389-396.

DEPARTMENT **MOBILITY & PUBLIC WORKS**
Flanders hydraulics Research

Berchemlei 115, 2140 Antwerp

T +32 (0)3 224 60 35

F +32 (0)3 224 60 36

waterbouwkundiglabo@vlaanderen.be

www.flandershydraulicsresearch.be